L.N.L. - I.N.F.N. (REP) 77 / 93

# A FIELD MODEL FOR ANALYSING WAVEGUIDE DC-BREAKS

C.T. Iatrou and M. Cavenago

*I.N.F.N. Laboratori Nazionali di Legnaro*

A cura del servizio
Documentazione dei
L.N.L.

# A FIELD MODEL FOR ANALYSING WAVEGUIDE DC-BREAKS

C. T. Iatrou and M. Cavenago

*Laboratori Nazionali di Legnaro-INFN*
*via Romea 4, I-35020 Legnaro (PD)*

*The problem of a rectangular waveguide open-junction which is fundamental in the design of dc-breaks is investigated using field theory and the relevant model of two, normally intersected, infinite parallel-planes waveguides. Approximate expressions are derived for the reflected, transmitted and radiated power, which are shown to be sufficiently reliable in a domain of practical interest, regarding the width and the dielectric loading of the gap. The analysis shows that a substantial fraction of the microwave power leaks from the dielectric gap, even for marginally small gaps, imposing the absolute necessity of using a choke-flange at the waveguide junction, to prevent microwave radiation, for safety reasons, and to improve transmission.*

## 1. INTRODUCTION

Frequently the coupling of two sections of a waveguide line is desired under circumstances that make the attainment of a good metallic contact rather difficult, or that even prohibit the contact because of electrical insulation reasons. A number of applications [1]-[2] require this type of coupling, such as rotary joints or other types of motional joints, frequently used in radar applications, switches, short-circuiting plungers, phase shifters, open-junctions allowing possible small misalignments in the rf-line components, and dc-breaks for dc electrical insulation between two parts of the rf-circuit without interrupting the rf-signal.

In ECR ion sources [3]-[8], the vessel is biased to a high potential of $10 \div 20$ kV, while the klystron amplifier, which feeds the plasma chamber with microwave power, and all the components of the waveguide line up to the chamber are earthed for economy and safety reasons. Thus, the waveguide line has to be electrically broken at a certain position before the plasma chamber using a dc-break [4].

In general, dc-breaks differ greatly from traditional microwave windows, because the high voltage between the two parts of the component does not allow any metallic contact, imposing a gap between them, which of course depends on the voltage to be sustained. Since there is no metallic continuity, the microwave power may be reflected and transmitted through the discontinuity, as in a common rf-window, but furthermore it may be radiated leaking out from the gap between the two parts. For better performance and in order to avoid sparks in the component, the gap is usually filled up with dielectric material and the dielectric sheet extends to greater radius than the metallic parts. The most important constrained parameter in the design

---

This work was partly supported by the European Economic Community under Contract ERBCHBGCT920207 of the "Human Capital and Mobility" program.

of a dc-break is the rf leakage from the gap between the two parts of the device. Calculations using a simplified field model [9] showed that an important fraction of the incoming microwave power may be radiated from the gap; geometric optics considerations led to a different result. A more precise and detailed approach is then advisable, in order to obtain more accurate results about the radiated power and to make a decision concerning a technologically feasible solution to the problem.

Our objective in this report is to produce analytical expressions for the reflected, transmitted, and radiated power through the dielectric gap of a dc-break, using field equations and a model of two, normally intersected, infinite parallel-planes waveguides. One of them represents the feeding waveguide, while the other one, which is assumed to be filled up with dielectric material, is the model of the gap between the two parts of an actual dc-break. In the second chapter of the report we describe the model in detail, along with the basic equations. In the third and fourth chapters we derive expressions for the Fourier coefficients of the two wave functions, from which the wave fields are generated. Finally in the last chapter we present the results of the numerical simulations, and we discuss about their reliability in different domains of width and dielectric loading of the gap.

## 2. MODEL AND BASIC EQUATIONS

In rectangular waveguides, the total electromagnetic field can always be decomposed into $\mathrm{TE}_{mn}$ and $\mathrm{TM}_{mn}$ modes, depending on whether the $E_z$ or the $B_z$ component vanishes. The subscripts $m$ and $n$ represent the number of half-period variations of the field along the transverse $x$ and $y$ coordinates respectively. By convention, the $x$ coordinate is assumed to coincide with the larger transverse dimension (Fig.1), so the $\mathrm{TE}_{10}$ mode has lower cut-off frequency than the $\mathrm{TE}_{01}$.

The field components of the $\mathrm{TE}_{mn}$ mode are:

$$B_z = B_0 \cos(k_x x) \cos(k_y y) \mathrm{e}^{-jkz} \tag{1a}$$

$$B_x = j \frac{k k_x}{k_c^2} B_0 \sin(k_x x) \cos(k_y y) \mathrm{e}^{-jkz} \tag{1b}$$

$$B_y = j \frac{k k_y}{k_c^2} B_0 \cos(k_x x) \sin(k_y y) \mathrm{e}^{-jkz} \tag{1c}$$

$$E_x = j \frac{\omega k_y}{k_c^2} B_0 \cos(k_x x) \sin(k_y y) \mathrm{e}^{-jkz} \tag{1d}$$

$$E_y = -j \frac{\omega k_x}{k_c^2} B_0 \sin(k_x x) \cos(k_y y) \mathrm{e}^{-jkz} \tag{1e}$$

where, $k_x = m\pi/b$ and $k_y = n\pi/a$ are the wavenumbers in the $x$ and $y$ coordinates,

$$k_c = \sqrt{k_x^2 + k_y^2} \tag{2a}$$

is the cut-off wavenumber,

$$k = \sqrt{\frac{\omega^2}{c^2} - k_c^2} \tag{2b}$$

is the guided wavenumber, $\omega = 2\pi f$ is the angular wave frequency, $c$ is the speed of light, and $a$, $b$ are the waveguide transverse dimensions in the $y$ and $x$ directions, with $b > a$.

For practical reasons in most experimental work with rectangular waveguides the dominant $TE_{10}$ mode is used. For this wave, substituting $m = 1$ and $n = 0$ in equations (1), the non-vanishing fields are:

$$B_z = B_0 \cos(k_x x) \mathrm{e}^{-jkz} \tag{3a}$$

$$B_x = jB_0 \frac{k}{k_x} \sin(k_x x) \mathrm{e}^{-jkz} \tag{3b}$$

$$E_y = -jB_0 \frac{\omega}{k_x} \sin(k_x x) \mathrm{e}^{-jkz} \tag{3c}$$

To simulate an open-junction between two rectangular waveguides of the same transverse dimensions ($a \times b$), we consider two, normally intersected, infinite parallel-planes waveguides, as shown in figure 2. The parallel planes of the horizontal waveguide are infinitely extended in the $x$ and $z$-directions, while the distance between them is taken equal to the small transverse dimension of the actual rectangular waveguides. As for the vertical one, which is assumed to be filled with dielectric material of relative permitivity $\epsilon_r$, the parallel plates are extended to infinity in the $x$ and $y$-directions, while the distance between them is $d$. The waves propagate in the horizontal guide in the $z$-direction, and in the vertical one in the $y$-direction.

The incoming wave is assumed to propagate along the horizontal guide to the positive $z$-direction, and at the junction it is divided into a reflected wave, travelling in the negative $z$-direction, a transmitted wave, travelling in the positive $z$-direction, and a radiated wave, which actually represents the leakage of the open-junction, travelling in the positive and negative $y$-directions. Since in the actual case of the rectangular waveguides, the incoming wave propagates in the dominant $TE_{10}$ mode, we will consider in our model waves with a harmonic variation in the $x$-direction, of the type $\exp(jk_x x)$, where $k_x = \pi/b$, with $b$ being the large transverse dimension of the actual rectangular guide. So, the extension of the waveguide planes to infinity in the $x$-direction is just a geometric simplification, since the type of the wave fields is that of a rectangular waveguide with $a$ and $b$, or $d$ and $b$ transverse dimensions.

As one can see from eqn.(3), the $TE_{10}$ mode has only the $E_y$ component, with no variation in the $y$-direction. For this reason, let us represent the electric field components $E_x$ and $E_z$ as the partial derivative on $y$ of two functions $\Phi$ and $X$, in the following way

$$E_x = \partial_y \Phi \tag{4}$$

and

$$E_z = \frac{1}{\epsilon_r} \partial_y X \tag{5}$$

where $\epsilon_r$ is the relative dielectric index; $\partial_a$ denotes the partial derivative with respect to any variable $a$. The third component of the electric field can be obtained, in terms of $\Phi$ and $X$ by applying Gauss's law $\nabla \cdot \vec{D} = 0$

$$E_y = -\partial_x \Phi - \frac{1}{\epsilon_r} \partial_z X \tag{6}$$

because $\epsilon_r$ does not depends on $x$ and $y$.

Then the incoming field of $TE_{10}$ mode corresponds to $\Phi$ and $X$ independent from $y$. Also, using Ampère's law, we compute the magnetic field components, as

$$B_x = -j \frac{1}{\omega} \left[ \partial_x \partial_z \Phi + \partial_z \left( \frac{1}{\epsilon_r} \partial_z X \right) + \frac{1}{\epsilon_r} \partial_y^2 X \right] \tag{4}$$

$$B_y = -j \frac{1}{\omega} \left( \partial_y \partial_z \Phi - \frac{1}{\epsilon_r} \partial_x \partial_y X \right) \tag{5}$$

$$B_z = j \frac{1}{\omega} \left[ \left( \partial_x^2 + \partial_y^2 \right) \Phi + \frac{1}{\epsilon_r} \partial_x \partial_z X \right] \tag{6}$$

Finally, using the Faraday's law we can easily show, that the functions $\Phi$ and $X$ satisfy the wave equation

$$\left( \epsilon_r \frac{\omega^2}{c^2} + \triangle \right) \Phi = 0 \tag{10a}$$

$$\left( \epsilon_r \frac{\omega^2}{c^2} + \triangle \right) X = 0 \tag{10b}$$

The major reason for $X$ and $\Phi$ definitions is their effectiveness in keeping equations simple, while reducing the degrees of freedom. Also, we note that $X/\epsilon_r$ enters in eqns.(4)-(6) as a flow potential for divergenceless fields in $xz$ plane, while $\Phi$ in $xy$ plane.

On the metallic boundary B1 (see figure 3), the following conditions must hold

$$E_x = 0 \quad \Rightarrow \quad \partial_y \Phi = 0 \tag{11a}$$

$$E_y = 0 \quad \Rightarrow \quad \partial_x \Phi + \frac{1}{\epsilon_r} \partial_z X = 0 \tag{11b}$$

$$B_z = 0 \quad \Rightarrow \quad \left( \partial_x^2 + \partial_y^2 \right) \Phi + \frac{1}{\epsilon_r} \partial_x \partial_z X = 0 \tag{11c}$$

Since this metallic wall B1 is infinitely extended in $x$ and $y$, we can differentiate boundary conditions with respect to $x$ and $y$; or even, we can integrate them on $x$ and $y$, since additional constants in $\Phi$ and $X$ are meaningless. Indeed, integrating (11a) on $y$ and substituting the result in (11b), we express these conditions (that must be satisfied by $\Phi$ and $X$, on the B1 boundary) as:

$$\Phi = 0 \tag{12a}$$

$$\frac{1}{\epsilon_r}\partial_z X = 0 \tag{12b}$$

By differentiating (11a) with respect to $y$ and eqn.(11b) with respect to $x$ we obtain (11c), which proves that only two indipendent boundary conditions exist.

On the metallic boundary B2 the following conditions must be satisfied

$$E_x = 0 \quad \Rightarrow \quad \partial_y \Phi = 0 \tag{13a}$$

$$E_z = 0 \quad \Rightarrow \quad \frac{1}{\epsilon_r}\partial_y X = 0 \tag{13b}$$

$$B_y = 0 \quad \Rightarrow \quad \partial_y \partial_z \Phi - \frac{1}{\epsilon_r}\partial_x \partial_y X = 0 \tag{13c}$$

Here conditions may be differentiated on $x$ and $z$. Equation (13c) is then a direct consequence of eqns.(13a) and (13b), which are therefore the two independent boundary conditions that $\Phi$ and $X$ must satisfy on B2.

On the interface between the two waveguides, the normal components of $\vec{D}$ and $\vec{B}$ and the tangential components of $\vec{E}$ and $\vec{B}$ must be continuous. So, using the notation "$f = \text{cont}$" to mean that $f(z)$ is continous at the air-dieletric interface, we can write

$$D_z = \text{cont} \quad \Rightarrow \quad \partial_y X = \text{cont} \tag{14a}$$

$$E_x = \text{cont} \quad \Rightarrow \quad \partial_y \Phi = \text{cont} \tag{14b}$$

$$E_y = \text{cont} \quad \Rightarrow \quad \partial_x \Phi + \frac{1}{\epsilon_r}\partial_z X = \text{cont} \tag{14c}$$

$$B_z = \text{cont} \quad \Rightarrow \quad \left(\partial_x^2 + \partial_y^2\right)\Phi + \frac{1}{\epsilon_r}\partial_x \partial_z X = \text{cont} \tag{14d}$$

$$B_x = \text{cont} \quad \Rightarrow \quad \frac{1}{\epsilon_r}\left(\partial_y^2 + \partial_z^2\right) X + \partial_x \partial_z \Phi = \text{cont} \tag{14e}$$

$$B_y = \text{cont} \quad \Rightarrow \quad \partial_y \partial_z \Phi - \frac{1}{\epsilon_r}\partial_x \partial_y X = \text{cont} \tag{14f}$$

Again, $\partial_x$ and $\partial_y$ may be applied to these conditions.

Then, by integrating (14b) on $y$, we obtain the following interface condition for the function $\Phi$

$$\Phi = \text{cont} \tag{15a}$$

Integrating (14f) on $y$ we get

$$\partial_z \Phi - \frac{1}{\epsilon_r}\partial_x X = \text{cont} \tag{15b}$$

The two interface conditions that must be satisfied by the $X$ function are obtained by integrating equation (14a) on $y$ and substituting $\Phi$ from (15a) to (14c),

$$X = \text{cont} \tag{16a}$$

$$\frac{1}{\epsilon_r}\partial_z X = \text{cont} \tag{16b}$$

Equation (14d) is the sum of $\partial_x^2 + \partial_y^2$ applied to (15a) and $\partial_x$ applied to (16b), therefore it adds no further information. Equation (14e) may be obtained by applying $\partial_x$ to (15b) and replacing $\partial_x^2 X$ by the field equation (10a), obtaining the intermediate equation:

$$\frac{1}{\epsilon_r}(\partial_y^2 + \partial_z^2)X + \frac{\omega^2}{c^2}X + \partial_z\partial_x\Phi = \text{cont}$$

which reduces to (14e) thanks to (16a).

Therefore the four linearly independent boundary conditions are (15) and (16). We note that $X$ is separated.

Let us now represent the function $\Phi$ and $X$, in the regions I and II (see figure 3), as infinite sums on Fourier components

$$X_{\text{I}} = \left[e^{jkz} + \sum_{m=0}^{\infty} a_{m_X} \cos(k_{ym}y)e^{k_{zm}z}\right] e^{jk_x x} \tag{17}$$

$$X_{\text{II}} = \sum_{m=0}^{\infty} b_{m_X} \cos(k_{ym}y)e^{-k_{zm}z}e^{jk_x x} \tag{18}$$

$$\Phi_{\text{I}} = \sum_{m=0}^{\infty} a_{m_\Phi} \cos(k_{ym}y)e^{k_{zm}z}e^{jk_x x} \tag{19}$$

$$\Phi_{\text{II}} = \sum_{m=0}^{\infty} b_{m_\Phi} \cos(k_{ym}y)e^{-k_{zm}z}e^{jk_x x} \tag{20}$$

where

$$k_x = \frac{\pi}{b}$$

$$k_{ym} = \frac{m\pi}{a}$$

$$k = \sqrt{\frac{\omega^2}{c^2} - k_x^2}$$

$$k_{zm} = \sqrt{k_{ym}^2 - k^2}$$

$$k_{z0} = -jk$$

Note that only the $X_{\text{I}}$ function contains a driving term, since waves are generated at $z = -\infty$, which excludes driving terms in $X_{\text{II}}$ and $\Phi_{\text{II}}$. Moreover, $\Phi_{\text{I}}$ needs not to contain a driving term, because the $X_{\text{I}}$ driving term is sufficient to reproduce the incoming $\text{TE}_{10}$ mode. The coefficients $a_{m_X}$ and $a_{m_\Phi}$ correspond to reflected waves, back to the region I, while the coefficients $b_{m_X}$ and $b_{m_\Phi}$ correspond to transmitted waves, through the open-junction to region II. The coefficients with subscript

"0" correspond to the dominant $TE_{10}$ mode, and hence to propagating waves, while the coefficients with subscript different than zero correspond to evanescent waves.

Since the $\Phi$ function does not contain any driving term, this function, and the corresponding waves, will be generated just because of the presence of the discontinuities at $z = 0$ and $z = d$. More precisely, on account of eqn.(15b), they will be generated only if there is a change in the dielectric constant at the discontinuities. Otherwise the quantity $\frac{1}{\epsilon_r}\partial_x X$ would be continuous, so that $\partial_z \Phi$ and $\Phi$ itself would be continuous at the interface; therefore, $\Phi$ would satisfy the equations of a damped resonator without internal discontinuities in the union of regions I, II, and III, with mixed boundary condition (=0); this would imply $\Phi = 0$.

In region III we represent the functions $\Phi$ and $X$ as Fourier integrals

$$X_{\mathrm{III}} = \int_{-\infty}^{+\infty} \frac{dk_y}{2\pi} e^{-jk_y y} \left[ c_X(k_y) e^{jk_z z} + d_X(k_y) e^{-jk_z z} \right] e^{jk_x x} \tag{21}$$

$$\Phi_{\mathrm{III}} = \int_{-\infty}^{+\infty} \frac{dk_y}{2\pi} e^{-jk_y y} \left[ c_\Phi(k_y) e^{jk_z z} + d_\Phi(k_y) e^{-jk_z z} \right] e^{jk_x x} \tag{22}$$

where

$$k' = \sqrt{\epsilon_r \frac{\omega^2}{c^2} - k_x^2}$$

$$k_z = \sqrt{k'^2 - k_y^2}$$

with the square root analytically continuated for non-positive arguments (the complex plane cut is yet to be defined, but we will see that the results do not depend on its choice).

The propagating waves $E_y$ and $B_x$ in regions I and II are given by

$$E_y^{\mathrm{I}} = -j \left[ e^{jkz} - \left( a_{0X} - \frac{k_x}{k} a_{0\Phi} \right) e^{-jkz} \right] e^{jk_x x} \tag{23a}$$

$$E_y^{\mathrm{II}} = -j \left( 1 + b_{0X} + \frac{k_x}{k} b_{0\Phi} \right) e^{jkz} e^{jk_x x} \tag{23b}$$

$$B_x^{\mathrm{I}} = j \frac{k}{\omega} \left[ e^{jkz} + \left( a_{0X} - \frac{k_x}{k} a_{0\Phi} \right) e^{-jkz} \right] e^{jk_x x} \tag{24a}$$

$$B_x^{\mathrm{II}} = j \frac{k}{\omega} \left( 1 + b_{0X} + \frac{k_x}{k} b_{0\Phi} \right) e^{jkz} e^{jk_x x} \tag{24b}$$

Thus the reflection ($\rho$) and transmission ($\tau$) coefficients in power, as well as the leakage ($R$), are given by the following formulas

$$\rho = \left( a_{0X} - \frac{k_x}{k} a_{0\Phi} \right) \left( a_{0X}^* - \frac{k_x}{k} a_{0\Phi}^* \right) \tag{25a}$$

$$\tau = \left(b_{0X} - \frac{k_x}{k} b_{0\Phi}\right)\left(b_{0X}^* - \frac{k_x}{k} b_{0\Phi}^*\right) \tag{25b}$$

$$R = 1 - \rho - \tau \geq 0 \tag{25c}$$

where by the superscript $*$ we denote complex conjugate quantities.

To compute these two coefficients, and hence the power which is radiated in the vertical waveguide, the Fourier coefficients $a_{0X}$, $a_{0\Phi}$, $b_{0X}$, and $b_{0\Phi}$ must be calculated. This is the subject of the following chapters.

## 3. COMPUTATION OF THE $X$-FUNCTION'S COEFFICIENTS

Using expressions (17), (18), and (21), the interface conditions (16) for the $X$ function at $z = 0$ and $z = d$ can be written as

$$1 + \sum_{m=0}^{\infty} a_{mX} \cos(k_{ym} y) = \int_{-\infty}^{+\infty} \frac{dk_y}{2\pi} e^{-jk_y y} \left[c_X(k_y) + d_X(k_y)\right] \tag{26a}$$

$$\sum_{m=0}^{\infty} b_{mX} \cos(k_{ym} y) e^{-k_{zm} d} = \int_{-\infty}^{+\infty} \frac{dk_y}{2\pi} e^{-jk_y y} \left[c_X(k_y) e^{jd\sqrt{k'^2 - k_y^2}} + d_X(k_y) e^{-jd\sqrt{k'^2 - k_y^2}}\right] \tag{26b}$$

$$\left(jk + \sum_{m=0}^{\infty} a_{mX} k_{zm} \cos(k_{ym} y)\right) \mathrm{I}(y) = j\frac{1}{\epsilon_r} \int_{-\infty}^{+\infty} \frac{dk_y}{2\pi} e^{-jk_y y} \sqrt{k'^2 - k_y^2} \left[c_X(k_y) - d_X(k_y)\right] \tag{26c}$$

$$\left(\sum_{m=0}^{\infty} b_{mX} k_{zm} \cos(k_{ym} y) e^{-k_{zm} d}\right) \mathrm{I}(y) = -j\frac{1}{\epsilon_r} \int_{-\infty}^{+\infty} \frac{dk_y}{2\pi} e^{-jk_y y} \sqrt{k'^2 - k_y^2} \left[c_X(k_y) e^{jd\sqrt{k'^2 - k_y^2}} - d_X(k_y) e^{-jd\sqrt{k'^2 - k_y^2}}\right] \tag{26d}$$

Equations (26a) and (26b) hold for $0 \leq y \leq a$; on the contrary, thanks to boundary conditions (12b), equations (26c) and (26d) hold for the whole real axis $-\infty < y < +\infty$, with $\mathrm{I}(y)$ being the indicatrix of the interval $0 \leq y \leq a$ (a function equal to 1 in the interval and zero elsewhere).

Multiplying eqns.(26a) and (26b) by $\cos(k_{yn} y')$ and integrating them from $y' = 0$ to $y' = a$, we obtain

$$\frac{1}{2}(1 + \delta_{n0}) a_{nX} = -\delta_{n0} + \frac{1}{a} \int_{-\infty}^{+\infty} \frac{dk_y}{2\pi} \left[c_X(k_y) + d_X(k_y)\right] \int_0^a dy' \cos(k_{yn} y') e^{-jk_y y'} \tag{27a}$$

$$\frac{1}{2}(1+\delta_{n0})b_{nx} = \frac{e^{k_{zn}d}}{a}\int_{-\infty}^{+\infty}\frac{dk_y}{2\pi}\left[c_X(k_y)e^{jd\sqrt{k'^2-k_y^2}} + d_X(k_y)e^{-jd\sqrt{k'^2-k_y^2}}\right]$$
$$\int_0^a dy'\cos(k_{yn}y')e^{-jk_y y'} \qquad (27b)$$

Then, we multiply eqns.(26c) and (26d) by $e^{jk'_y y}$, and we integrate them from $y=-\infty$ to $y=+\infty$, to get

$$c_X(k_y) - d_X(k_y) = \frac{\epsilon_r k}{\sqrt{k'^2-k_y^2}}\int_0^a dy e^{jk_y y}$$
$$-j\frac{\epsilon_r}{\sqrt{k'^2-k_y^2}}\sum_{m=0}^{\infty} a_{mx}\,k_{zm}\int_0^a dy\cos(k_{ym}y)e^{jk_y y} \qquad (28a)$$

$$c_X(k_y)e^{jd\sqrt{k'^2-k_y^2}} - d_X(k_y)e^{-jd\sqrt{k'^2-k_y^2}} = j\frac{\epsilon_r k}{\sqrt{k'^2-k_y^2}}\sum_{m=0}^{\infty} b_{mx}\,k_{zm}e^{-k_{zm}d}$$
$$\int_{-\infty}^{+\infty} dy\cos(k_{ym}y)e^{jk_y y} \qquad (28b)$$

We can solve eqns.(28) for $c_X(k_y)$ and $d_X(k_y)$ and substitute the result in eqns.(27). In detail, multiplying eqn.(28a) by $-e^{-jd\sqrt{k'^2-k_y^2}}$ and adding the result with eqn.(28b) we obtain an expression for the coefficient $c_X(k_y)$ in terms of the coefficients $a_{mx}$ and $b_{mx}$. A similar expression for the coefficient $d_X(k_y)$ may be obtained by multiplying eqn.(28a) by $e^{jd\sqrt{k'^2-k_y^2}}$, and then substracting the result from eqn.(28b). Then, using these expression we can compute the quantities

$$c_X(k_y) + d_X(k_y)$$

and

$$c_X(k_y)e^{jd\sqrt{k'^2-k_y^2}} + d_X(k_y)e^{-jd\sqrt{k'^2-k_y^2}}$$

and by substituting them into eqns.(27), we obtain the following system for the $X$-function's Fourier coefficients

$$\frac{1}{2}(1+\delta_{n0})a_{nx} + \frac{\epsilon_r}{a}\sum_{m=0}^{\infty} k_{zm}\left(I_{nm}a_{mx} + 2e^{-k_{zm}d}J_{nm}b_{mx}\right) = -\delta_{n0} - j\frac{\epsilon_r k}{a}I_{n0} \qquad (29)$$

$$\frac{1}{2}(1+\delta_{n0})b_{nx} + \frac{\epsilon_r e^{k_{zn}d}}{a}\sum_{m=0}^{\infty} k_{zm}\left(2J_{nm}a_{mx} + e^{-k_{zm}d}I_{nm}b_{mx}\right) = -j2\frac{\epsilon_r k}{a}e^{k_{zn}d}J_{n0} \qquad (30)$$

where $I_{nm}$ and $J_{nm}$ are the following integrals

$$I_{nm} = -d \int_{-\infty}^{+\infty} \frac{dk_y}{2\pi} \frac{\cot\left(d\sqrt{k'^2 - k_y^2}\right)}{d\sqrt{k'^2 - k_y^2}} \int_0^a dy \cos(k_{ym}y) e^{jk_y y} \int_0^a dy' \cos(k_{ym}y') e^{-jk_y y'} \tag{31a}$$

$$J_{nm} = -\frac{d}{2} \int_{-\infty}^{+\infty} \frac{dk_y}{2\pi} \frac{\csc\left(d\sqrt{k'^2 - k_y^2}\right)}{d\sqrt{k'^2 - k_y^2}} \int_0^a dy \cos(k_{ym}y) e^{jk_y y} \int_0^a dy' \cos(k_{ym}y') e^{-jk_y y'} \tag{31b}$$

which actually express the coupling between different modes (evanescent and the propagating one) due to the existence of the discontinuities at $z = 0$ and $z = d$.

The above integrals have been analytically computed using the methods of contour integration in the complex plane, and the complete analysis is given in the Appendix. However, let us discuss here some qualitative topics of the problem. First, the integrand is even in $\sqrt{k'^2 - k_y^2}$, so that only the square of this radical and not the radical itself appears in any power series expansion of the integrand; this makes immaterial the choice of the cut in the complex plane for the square root immaterial. Moreover, it is easily seen from expressions (31), that both integrals have an infinite number of poles in the complex plane. A pair of poles lies on the real axis, at $k_y = \pm k'$, and infinite pairs of poles are at $k_y = \pm jk_\ell$, where $k_\ell = [(\ell^2\pi^2/d^2) - k'^2]^{1/2}$ with $\ell \geq 1$; For small values of $d$ these poles are completely imaginary. The real pair of poles at $k'$ corresponds to the dominant $\mathrm{TE}_{10}$ mode, which is always propagating in the dielectric waveguide. The $k_\ell$ poles correspond to $\mathrm{TE}_{1\ell}$ and $\mathrm{TM}_{1\ell}$ modes, which may be evanescent or propagating, depending on the transverse dimension $d$ of the dielectric waveguide. For small values of $d$, these modes are evanescent, and they begin to propagate as $d$ becomes greater than $\ell\pi/k'$, for each value of $\ell$.

It is worthwhile to discuss the meaning of results (unphysical) if singularities in the integrand are fixed by taking the Principal Value. The introduction of the result found in that way into eqns.(29) and (30) led to a system of equations with such a structure imposing always a solution satisfying the identity

$$\rho + \tau = 1$$

which, physically, means that there is no power radiated into the vertical waveguide, whatever the value of $d$. A way to interpret physically this result is to consider that there are, indeed, waves propagating into the vertical waveguide, but these waves are subject to reflections from the boundaries at $y = \pm\infty$. Thus, no power is lost from the horizontal waveguide.

A simple way to avoid this unphysical situation is to introduce a small damping to the waves that travel along the vertical waveguide. The introduction, for instance, of a small imaginary part in the dielectric constant, that characterizes the medium filling up the vertical waveguide, will cause power absorption from the medium. In

this way, the power flows into the vertical waveguide, is dumped as it travels along it, and thus it does not reach the "borders" at $y = \pm\infty$ to be reflected back. In mathematical terms, we evaluated the integrals (31) by the residue method, keeping always an imaginary part $\eta < 0$ for the relative dielectric constant ($\epsilon_r \to \epsilon_r + j\eta$). In the complex plane, the pair of the previously real poles at $k_y = \pm k'$ is now displaced from the real axis, acquiring an imaginary part proportional to $\eta$. Likewise, the infinite pairs of the previously purely imaginary poles at $k_y = \pm j k_\ell$ are now displaced from the imaginary axis, due to a real part, proportional to $\eta$. The method is completely similar to the "Landau prescription" for the choice of the path of integration in instability studies, whereas the imaginary part added to $\omega \to \omega_r - j\eta$ is motivated there by adiabatic growth.

From eqn.(A8), taking the limit as $\eta \to 0$, we found for the integrals (31) the final result: if $(-1)^n = (-1)^m$

$$I_{nm} = (g'_n + \sum_{\ell=1}^{\infty} g_{n\ell})\delta_{nm} + \frac{c'}{(s'^2 - n^2)(s'^2 - m^2)} + \sum_{\ell=1}^{\infty} \frac{(-1)^\ell c_\ell}{(s_\ell^2 + n^2)(s_\ell^2 + m^2)} \tag{32a}$$

$$2J_{nm} = (g'_n - \sum_{\ell=1}^{\infty} g_{n\ell})\delta_{nm} + \frac{c'}{(s'^2 - n^2)(s'^2 - m^2)} - \sum_{\ell=1}^{\infty} \frac{(-1)^\ell c_\ell}{(s_\ell^2 + n^2)(s_\ell^2 + m^2)} \tag{32b}$$

and if $(-1)^n = -(-1)^m$

$$I_{nm} = J_{nm} = 0 \tag{32c}$$

Here, we use the notations

$$g'_n = -\frac{a^3}{2d\pi^2(s'^2 - n^2)} \tag{33a}$$

$$g_{n\ell} = \frac{a^3}{d\pi^2(s_\ell^2 + n^2)} \tag{33b}$$

$$s' = \frac{k'a}{\pi} \tag{33c}$$

$$s_\ell = \frac{k_\ell a}{\pi} \tag{33d}$$

$$k_\ell = \sqrt{\frac{\ell^2\pi^2}{d^2} - k'^2} \tag{33e}$$

$$c' = j\frac{a^3 s'}{d\pi^3}(1 - e^{j\pi s'}) \tag{33f}$$

$$c_\ell = 2\frac{a^3 s_\ell}{d\pi^3}(1 - e^{-\pi s_\ell}) \tag{33g}$$

In the above expressions, primed quantities refer to the $\pm k'$ poles of the integrals (31), while those with subscript $\ell$ to the $k_\ell$ poles. For small values of $d$

($d \leq \pi/2k'$), the main contribution to the integrals (32) comes from the $k'$ poles, while the significance of the $k_\ell$ poles is increasing with increasing $d$. For this reason, it is enough to keep only the first ($\ell = 1$) term of the infinite summation in expression (32) for the rest of the analysis, assuming that we will restrict the applicability of the resulting formulas in values of $d$ which are not considerably greater than $\pi/2k'$. Thus, substituting (32) into (29) and (30), we note that the coefficients $a_{nx}$ and $b_{nx}$ with $n$ odd are zero, and we obtain the following system for the $X$-function's even order Fourier coefficients

$$D_{1nx}\, a_{nx} + D_{2nx}\, e^{-k_{zn}d} b_{nx} = -\left( \frac{A_X + B_X}{s'^2 - n^2} - \frac{C_X - D_X}{s_1^2 + n^2} + e_{nx} \right) \tag{34a}$$

$$D_{2nx}\, e^{k_{zn}d} a_{nx} + D_{1nx}\, b_{nx} = -\left( \frac{A_X + B_X}{s'^2 - n^2} + \frac{C_X - D_X}{s_1^2 + n^2} + f_{nx} \right) e^{k_{zn}d} \tag{34b}$$

where

$$D_{1nx} = \frac{1}{2}(1 + \delta_{n0}) + \frac{\epsilon_r}{a} k_{zn} (g'_n + g_{n1}) \tag{35a}$$

$$D_{2nx} = \frac{\epsilon_r}{a} k_{zn} (g'_n - g_{n1}) \tag{35b}$$

$$e_{nx} = \delta_{n0} + j\frac{\epsilon_r}{a} k \left[ (g'_n + g_{n1})\delta_{n0} + \frac{c'}{s'^2(s'^2 - n^2)} - \frac{c_1}{s_1^2(s_1^2 - n^2)} \right] \tag{35c}$$

$$f_{nx} = j\frac{\epsilon_r}{a} k \left[ (g'_n - g_{n1})\delta_{n0} + \frac{c'}{s'^2(s'^2 - n^2)} + \frac{c_1}{s_1^2(s_1^2 - n^2)} \right] \tag{35d}$$

Here $A_X$, $B_X$, $C_X$, and $D_X$ are the projections of $a_{nx}$ and $b_{nx}$ onto the notable axes of $I_{nm}$ and $J_{nm}$ which can be seen from eqn.(32) itself (these axes are embedded in the infinite dimension space $\{a_{nx}\}$, $\{b_{nx}\}$):

$$A_X = \frac{\epsilon_r}{a} c' \sum_{m=0}^{\infty} \frac{k_{zm}}{(s'^2 - m^2)} a_{mx} \tag{35e}$$

$$B_X = \frac{\epsilon_r}{a} c' \sum_{m=0}^{\infty} \frac{k_{zm} e^{-k_{zm}d}}{(s'^2 - m^2)} b_{mx} \tag{35f}$$

$$C_X = \frac{\epsilon_r}{a} c_1 \sum_{m=0}^{\infty} \frac{k_{zm}}{(s_1^2 + m^2)} a_{mx} \tag{35g}$$

$$D_X = \frac{\epsilon_r}{a} c_1 \sum_{m=0}^{\infty} \frac{k_{zm} e^{-k_{zm}d}}{(s_1^2 + m^2)} b_{mx} \tag{35h}$$

with the sums restricted to even values of the index $m$, for the rest of the chapter.

The infinite system (34) can be solved. Indeed, we note that a system of four equations may be derived for the unknowns $A_X$, $B_X$, $C_X$, and $D_X$, which is the core system of our problem. In detail, from the system (34) we obtain expressions

for the coefficients $a_{nX}$ and $b_{nX}$ in terms of $A_X$, $B_X$, $C_X$, and $D_X$, and then we introduce them into (35e)-(35h) to get the system

$$A_X = -H_X A_X - H_X B_X + \frac{c'}{c_1} G_X C_X - \frac{c'}{c_1} G_X D_X + F_{1X} \tag{36a}$$

$$B_X = -H_X A_X - H_X B_X - \frac{c'}{c_1} G_X C_X + \frac{c'}{c_1} G_X D_X - F_{2X} \tag{36b}$$

$$C_X = -\frac{c_1}{c'} H_X A_X - \frac{c_1}{c'} H_X B_X + G_X C_X - G_X D_X + F_{3X} \tag{36c}$$

$$D_X = -\frac{c_1}{c'} H_X A_X - \frac{c_1}{c'} H_X B_X - G_X C_X + G_X D_X + F_{4X} \tag{36d}$$

where

$$H_X = \frac{\epsilon_r}{a} c' \sum_{m=0}^{\infty} \frac{k_{zm}}{(s'^2 - m^2)^2} \frac{D_{1mX} - D_{2mX}}{D_{mX}}$$

$$G_X = \frac{\epsilon_r}{a} c_1 \sum_{m=0}^{\infty} \frac{k_{zm}}{(s_1^2 + m^2)^2} \frac{D_{1mX} + D_{2mX}}{D_{mX}}$$

$$F_{1X} = -\frac{\epsilon_r}{a} c' \sum_{m=0}^{\infty} \frac{k_{zm}}{s'^2 - m^2} \frac{D_{1mX} e_{mX} - D_{2mX} f_{mX}}{D_{mX}}$$

$$F_{2X} = -\frac{\epsilon_r}{a} c' \sum_{m=0}^{\infty} \frac{k_{zm}}{s'^2 - m^2} \frac{D_{1mX} f_{mX} - D_{2mX} e_{mX}}{D_{mX}}$$

$$F_{3X} = -\frac{\epsilon_r}{a} c_1 \sum_{m=0}^{\infty} \frac{k_{zm}}{s_1^2 + m^2} \frac{D_{1mX} e_{mX} - D_{2mX} f_{mX}}{D_{mX}}$$

$$F_{4X} = -\frac{\epsilon_r}{a} c_1 \sum_{m=0}^{\infty} \frac{k_{zm}}{s_1^2 + m^2} \frac{D_{1mX} f_{mX} - D_{2mX} e_{mX}}{D_{mX}}$$

In the above expressions $D_{mX}$ is the determinant of the system (34).

The system (36) is easily decoupled into two independent equations, which are then solved to give

$$A_X + B_X = \frac{F_{1X} + F_{2X}}{1 + 2H_X} \tag{37a}$$

and

$$C_X - D_X = \frac{F_{3X} - F_{4X}}{1 - 2G_X} \tag{37b}$$

Having computed the infinite sums $A_X + B_X$ and $C_X - D_X$, we introduce them back into (34), and applying it for $n = 0$, we obtain the following expressions for the $X$-function's Fourier coefficients

$$a_{0X} = -\frac{D_{10X} - D_{20X}}{s'^2 D_{0X}} \frac{F_{1X} + F_{2X}}{1 + 2H_X} + \frac{D_{10X} + D_{20X}}{s_1^2 D_{0X}} \frac{F_{3X} - F_{4X}}{1 - 2G_X} - \frac{D_{10X} e_{0X} - D_{20X} f_{0X}}{D_{0X}} \tag{38a}$$

$$b_{0X} = \Big( -\frac{D_{10X} - D_{20X}}{s'^2 D_{0X}} \frac{F_{1X} + F_{2X}}{1 + 2H_X} - \frac{D_{10X} + D_{20X}}{s_1^2 D_{0X}} \frac{F_{3X} - F_{4X}}{1 - 2G_X} - \frac{D_{10X} f_{0X} - D_{20X} e_{0X}}{D_{0X}} \Big) e^{-jkz} \qquad (38b)$$

In the special case where there is no dielectric material filling up the vertical waveguide, the $X$ function alone sufficies for the determination of the reflection and transmission coefficients in power, which are given by

$$\rho = a_{0X}\, a_{0X}^* \qquad (39a)$$

and

$$\tau = b_{0X}\, b_{0X}^* \qquad (39b)$$

If the vertical waveguide is filled by a dielectric material, it is necessary to compute the $\Phi$-function's Fourier coefficients, and then to use eqns.(25) to find the total reflection and transmission coefficients.

## 4. COMPUTATION OF THE $\Phi$-FUNCTION'S COEFFICIENTS

Using expressions (19), (20), and (22), the interface conditions (15) for the $\Phi$-function at $z = 0$ and $z = d$ can be written in the following way

$$\sum_{m=0}^{\infty} a_{m\Phi} \cos(k_{ym} y) = \int_{-\infty}^{+\infty} \frac{dk_y}{2\pi} e^{-jk_y y} \Big[ c_\Phi(k_y) + d_\Phi(k_y) \Big] \qquad (40a)$$

$$\sum_{m=0}^{\infty} b_{m\Phi} \cos(k_{ym} y) e^{-k_{zm} d} = \int_{-\infty}^{+\infty} \frac{dk_y}{2\pi} e^{-jk_y y} \Big[ c_\Phi(k_y) e^{jd\sqrt{k'^2 - k_y^2}} + d_\Phi(k_y) e^{-jd\sqrt{k'^2 - k_y^2}} \Big] \qquad (40b)$$

$$\mathrm{I}(y) \sum_{m=0}^{\infty} a_{m\Phi} k_{zm} \cos(k_{ym} y) = jk_x \left( 1 - \frac{1}{\epsilon_r} \right) \left[ 1 + \sum_{i=0}^{\infty} a_{iX} \cos(k_{yi} y) \right] + j \int_{-\infty}^{+\infty} \frac{dk_y}{2\pi} e^{-jk_y y} \sqrt{k'^2 - k_y^2} \Big[ c_\Phi(k_y) - d_\Phi(k_y) \Big] \qquad (40c)$$

$$\mathrm{I}(y) \sum_{m=0}^{\infty} b_{m\Phi} k_{zm} \cos(k_{ym} y) e^{-k_{zm} d} = -jk_x \left( 1 - \frac{1}{\epsilon_r} \right) \sum_{i=0}^{\infty} b_{iX} \cos(k_{yi} y) e^{-k_{zi} d} - j \int_{-\infty}^{+\infty} \frac{dk_y}{2\pi} e^{-jk_y y} \sqrt{k'^2 - k_y^2} \Big[ c_\Phi(k_y) e^{jd\sqrt{k'^2 - k_y^2}} - d_\Phi(k_y) e^{-jd\sqrt{k'^2 - k_y^2}} \Big] \qquad (40d)$$

Equations (40a) and (40b) hold for $0 \leq y \leq a$; because of the boundary conditions, equations (40c) and (40d) hold for the whole real axis $-\infty < y < +\infty$, with I($y$) being the indicatrix of the interval $0 \leq y \leq a$.

Following the same procedure as in the case of the $X$-function, we obtain a similar system for the $\Phi$-function's Fourier coefficents

$$D_{1n_\Phi} a_{n_\Phi} + D_{2n_\Phi} e^{-k_{zn}d} b_{n_\Phi} = -\left( \frac{A_\Phi + B_\Phi}{s'^2 - n^2} - \frac{C_\Phi - D_\Phi}{s_1^2 + n^2} + e_{n_\Phi} \right) \tag{41a}$$

$$D_{2n_\Phi} e^{k_{zn}d} a_{n_\Phi} + D_{1n_\Phi} b_{n_\Phi} = -\left( \frac{A_\Phi + B_\Phi}{s'^2 - n^2} + \frac{C_\Phi - D_\Phi}{s_1^2 + n^2} + f_{n_\Phi} \right) e^{k_{zn}d} \tag{41b}$$

where

$$D_{1n_\Phi} = \frac{1}{2}(1 + \delta_{n0}) + \frac{k_{zn}}{a}(g'_n + g_{n1}) \tag{42a}$$

$$D_{2n_\Phi} = \frac{k_{zn}}{a}(g'_n - g_{n1}) \tag{42b}$$

$$\begin{aligned} e_{n_\Phi} = -j\frac{k_x(1-\epsilon_r^{-1})}{a} \Bigg\{ & \left[ (g'_n + g_{n1}) a_{nx} - (g'_n - g_{n1}) e^{-k_{zn}d} b_{nx} \right] \\ & + \sum_{p=0}^{\infty} \Bigg[ \frac{c'}{(s'^2 - n^2)(s'^2 - p^2)} (a_{px} - e^{-k_{zm}d} b_{px}) \\ & - \frac{c_1}{(s_1^2 + n^2)(s_1^2 + p^2)} (a_{px} + e^{-k_{zm}d} b_{px}) \Bigg] \Bigg\} \end{aligned} \tag{42c}$$

$$\begin{aligned} f_{n_\Phi} = -j\frac{k_x(1-\epsilon_r^{-1})}{a} \Bigg\{ & \left[ (g'_n - g_{n1}) a_{nx} - (g'_n + g_{n1}) e^{-k_{zn}d} b_{nx} \right] \\ & + \sum_{p=0}^{\infty} \Bigg[ \frac{c'}{(s'^2 - n^2)(s'^2 - p^2)} (a_{px} - e^{-k_{zm}d} b_{px}) \\ & + \frac{c_1}{(s_1^2 + n^2)(s_1^2 + p^2)} (a_{px} + e^{-k_{zm}d} b_{px}) \Bigg] \Bigg\} e^{k_{zn}d} \end{aligned} \tag{42d}$$

and notable axes projections

$$A_\Phi = \frac{1}{a} c' \sum_{m=0}^{\infty} \frac{k_{zm}}{(s'^2 - m^2)} a_{m_\Phi} \tag{42e}$$

$$B_\Phi = \frac{1}{a} c' \sum_{m=0}^{\infty} \frac{k_{zm} e^{-k_{zm}d}}{(s'^2 - m^2)} b_{m_\Phi} \tag{42f}$$

$$C_\Phi = \frac{1}{a} c_1 \sum_{m=0}^{\infty} \frac{k_{zm}}{(s_1^2 + m^2)} a_{m_\Phi} \tag{42g}$$

$$D_\Phi = \frac{1}{a} c_1 \sum_{m=0}^{\infty} \frac{k_{zm} e^{-k_{zm} d}}{(s_1^2 + m^2)} b_{m_\Phi} \tag{42h}$$

The fact that $\Phi$ is mastered by $X$ is evident from the presence of $a_{n_X}$ and $b_{n_X}$ in the expressions of the nonhomogeneous terms $e_{n_\Phi}$ and $f_{n_\Phi}$. As in the previous case of $X$ function, the system (41) is solvable after the core system for $A_\Phi$, $B_\Phi$, $C_\Phi$, and $D_\Phi$, which are functions of the unknown coefficients $a_{n_\Phi}$ and $b_{n_\Phi}$, is solved. Following the same procedure as in the case of the $X$ function, the quantities $A_\Phi + B_\Phi$ and $C_\Phi - D_\Phi$ are computed

$$A_\Phi + B_\Phi = \frac{F_{1_\Phi} + F_{2_\Phi}}{1 + 2H_\Phi} \tag{43a}$$

and

$$C_\Phi - D_\Phi = \frac{F_{3_\Phi} - F_{4_\Phi}}{1 - 2G_\Phi} \tag{43b}$$

where

$$H_\Phi = \frac{1}{a} c' \sum_{m=0}^{\infty} \frac{k_{zm}}{(s'^2 - m^2)^2} \frac{D_{1m_\Phi} - D_{2m_\Phi}}{D_{m_\Phi}}$$

$$G_\Phi = \frac{1}{a} c_1 \sum_{m=0}^{\infty} \frac{k_{zm}}{(s_1^2 + m^2)^2} \frac{D_{1m_\Phi} + D_{2m_\Phi}}{D_{m_\Phi}}$$

$$F_{1_\Phi} = -\frac{1}{a} c' \sum_{m=0}^{\infty} \frac{k_{zm}}{s'^2 - m^2} \frac{D_{1m_\Phi} e_{m_\Phi} - D_{2m_\Phi} f_{m_\Phi}}{D_{m_\Phi}}$$

$$F_{2_\Phi} = -\frac{1}{a} c' \sum_{m=0}^{\infty} \frac{k_{zm}}{s'^2 - m^2} \frac{D_{1m_\Phi} f_{m_\Phi} - D_{2m_\Phi} e_{m_\Phi}}{D_{m_\Phi}}$$

$$F_{3_\Phi} = -\frac{1}{a} c_1 \sum_{m=0}^{\infty} \frac{k_{zm}}{s_1^2 + m^2} \frac{D_{1m_\Phi} e_{m_\Phi} - D_{2m_\Phi} f_{m_\Phi}}{D_{m_\Phi}}$$

$$F_{4_\Phi} = -\frac{1}{a} c_1 \sum_{m=0}^{\infty} \frac{k_{zm}}{s_1^2 + m^2} \frac{D_{1m_\Phi} f_{m_\Phi} - D_{2m_\Phi} e_{m_\Phi}}{D_{m_\Phi}}$$

We also mention here that the above sums are to be restricted for even values of the index $m$ only.

Finally, we introduce the sums $A_\Phi + B_\Phi$ and $C_\Phi - D_\Phi$ into (41), and applying it for $n = 0$, we obtain the following expressions for the $\Phi$-function's Fourier coefficients

$$a_{0_\Phi} = -\frac{D_{10_\Phi} - D_{20_\Phi}}{s'^2 D_{0_\Phi}} \frac{F_{1_\Phi} + F_{2_\Phi}}{1 + 2H_\Phi} + \frac{D_{10_\Phi} + D_{20_\Phi}}{s_1^2 D_{0_\Phi}} \frac{F_{3_\Phi} - F_{4_\Phi}}{1 - 2G_\Phi} - \frac{D_{10_\Phi} e_{0_\Phi} - D_{20_\Phi} f_{0_\Phi}}{D_{0_\Phi}} \tag{44a}$$

$$b_{0_\Phi} = \Big( -\frac{D_{10_\Phi} - D_{20_\Phi}}{s'^2 D_{0_\Phi}} \frac{F_{1_\Phi} + F_{2_\Phi}}{1 + 2H_\Phi} - \frac{D_{10_\Phi} + D_{20_\Phi}}{s_1^2 D_{0_\Phi}} \frac{F_{3_\Phi} - F_{4_\Phi}}{1 - 2G_\Phi} - \frac{D_{10_\Phi} f_{0_\Phi} - D_{20_\Phi} e_{0_\Phi}}{D_{0_\Phi}} \Big) e^{-jkz} \qquad (44b)$$

From the coefficients of the $X$ and $\Phi$ functions given by expressions (38) and (44), the total reflection and transmission coefficients,as well as the leakage from a dc-break, may now be computed using eqns.(25).

## 5. NUMERICAL RESULTS AND DISCUSSION

In this chapter the analytical results of the previous chapters will be applied to simulate the dc-break between two WR-62 rectangular waveguides, operating at 14.4 GHz. The transverse dimensions of such a waveguide are: $a$=7.9 mm, and $b$=15.8 mm. The distance between the two waveguides will be denoted by $d$.

In Fig.4 we present the reflection and transmission coefficients, as well as the leakage of such a dc-break, as a function of the gap width $d$. The gap is assumed to be filled up with teflon, a dielectric material with a relative index $\epsilon_r = 2.1$. The most important parameter in the design of a dc-break is the amount of microwave power that is radiated from the gap (leakage). As it can be seen from Fig.4, the leakage is a rapidly growing function of $d$, for small values of $d$, reaching the maximum value of 53% at $d = 5.1$ mm. Even at $d = 1$ mm, which is actually a reasonable width for the gap of a dc-break operating at dc-voltages up to 20 KV, the leakage has been found to be as much as 33%, a value that imposes a detailed and careful design of the choke-flange, which will be used for the connection of the two waveguides, in order to avoid high levels of radiated power from the gap (the use of a carefully designed choke-flange will also increase the percentage of the transmitted power, from the moderate value of 63% to something about 95%, since it will not introduce but a small reactive component across the gap, affecting in that way slighly the reflected power [10]). Regarding the reflection and transmission coefficients, one can say that they have a smooth variation with $d$, up to a gap of 6 mm. For even wider gaps, the reflected and transmitted power have been found to oscillate sharply. This behaviour may be explained by considering the growing contribution of the $k_1$ poles in the expressions (32) for the integrals $I_{nm}$ and $J_{nm}$.

In Fig.5 we present the same curves, as Fig.4, in the case where the $k_1$ poles are not taken into account. As one can see by comparing with Fig.4, the curves have the same form, for values of $d$ smaller than 6 mm. For gaps wider than 6 mm, they continue their smooth variation with $d$, proving that the oscillating part of the reflected and transmitted power in Fig.4 is indeed an effect of the $k_1$ poles. For $d \leq 3$ mm, the curves of Fig.5 fit well with those of Fig.4, especially the one corresponding to the leakage. At $d = 1$ mm, the contribution of $k_1$ poles is not greater than 5%. In general, the comparison of these two figures offers a strong argument for the validity of our results, in the case where the width of the gap is kept smaller than 6 mm. For greater values of $d$, one should take into consideration the contribution of

further and further imaginary poles $k_\ell$, in the computation of the integrals $I_{nm}$ and $J_{nm}$; in order to find the complete solution to the problem one has to solve a system similar to (34), with sum on $\ell$ poles, a task which requires extremely heavy algebraic and computational manipulations to be carried out . Anyway, the use of dc-break's gaps wider than 3 mm or even 4 mm is considered out of question, because it would be extremely difficult to design a choke-flange with such a wide gap, to join the guides. In other words, no one can doubt that a 4 mm gap out of 8 mm waveguide will radiate no matter how sophisticated and detailed the design could be.

The influence of the $\Phi$-function can be investigated through the comparison of Figs.4 and 6. In Fig.6 the curves of the reflected, transmitted and radiated power are presented, taking into account only the $X$-function's reflection and transmission coefficients. The contribution of the $\Phi$-function's coefficients is not significant, especially as regards the radiated power, due to the relatively small value of the dielectric index of the teflon. As it is already mentioned, responsible for the generation of the $\Phi$-function and the corresponding waves is not the existence of the gap, but the discontinuity of the dielectric constant. Thus, since the gap is relatively lightly loaded by the teflon, the $\Phi$-function is slightly generated, contributing by a small amount to the total reflection and transmission coefficients.

Apart from the width $d$ of the gap, the second parameter that influences the operation of a dc-break, is the dielectric constant of the material filling up this gap. The reflected, transmitted and radiated power as functions of the relative index $\epsilon_r$, are presented in Figs.7 and 8. In Fig.7 both the $X$ and $\Phi$-functions are taken into account, while in Fig.8 only the contribution of the $X$-function is considered. The width of the gap is fixed at $d = 1$ mm. As it can be seen easily from these figures, the influence of the $\Phi$-function becomes important for large values of the dielectric index. For instance, at $\epsilon_r = 2.5$ the most affected coefficient is that of the reflection, by 10%., while at $\epsilon_r = 10$ the same coefficient is affected by at least 35%. Also, the leakage, computed without the $\Phi$-function's coefficients, has been found to be the 2/3 of the leakage computed with $X$ and $\Phi$-functions. At this value of $\epsilon_r$, the half-wavelength of the $TE_{10}$ mode in the gap is 3.37 mm, and thus the width of the gap is already the 1/3 of it, approaching the limits of the validity of our results. The radiated power increases from 27.7% at $\epsilon_r = 1$ to 34.5% at $\epsilon_r = 5.5$, and then it decreases to 25% at $\epsilon_r = 25$. The transmitted power decreases for small values of the dielectric index, from 69.3% at $\epsilon_r = 1$ to 62.8% at $\epsilon_r = 3$, and then it remains almost constant until $\epsilon_r = 13$. The reflected power remains almost constant, around the value of 3.5%, in a wide range of dielectric indices, up to $\epsilon_r = 10$.

In Fig.9 we present the same quantities as in Figs.7 and 8, but in their computation we take into account only the $k'$ poles of the integrals $I_{nm}$ and $J_{nm}$. As it can be seen by comparing Figs.7 and 9, the contribution of the $k_1$ poles is not significant for moderate values of the dielectric constant, as it was expected. The curves fit well for values of $\epsilon_r$ up to 12, within an error of less than 30%. For more heavy dielectric loads, the width of the gap (1 mm) becomes a considerable fraction of the half-wavelength of the $TE_{10}$ mode in the gap, and thus the contribution of the $k_1$ and probably of the rest of the $k_\ell$ poles becomes significant. Consequently, at this

specific value of 1 mm for the width of the gap, one could say that, our approximate solution gives reliable results for values of the dielectric constant up to 10 or 12.

## 6. CONCLUSIONS

A rectangular waveguide dc-break has been investigated, through an analytical model of an open-junction of two infinite parallel-plate waveguides. The complete field model has been used, and expressions have been derived for the coefficients of the reflected and transmitted power through the gap of the open-junction, including the effect of the propagating and the first evanescent mode in the dielectric slab, in terms of the Fourier coefficients of two wave functions $X$ and $\Phi$, which are used in the expressions of the wave fields. The numerical simulation of the dc-break showed that the expressions derived from the analysis are reliable in a certain range of gap's widths and dielectric loads of the gap. The criterion for the validity of our results is the width $d$ of the gap to remain smaller than the $1/4$ of the cutoff wavelength of the dominant $TE_{10}$ mode in the dielectric gap ($b \times d$) waveguide. For instance, in the case of a WR-62 dc-break, at 14.4 GHz, loading the gap with teflon, which has a dielectric constant equal to 2.1, the width of the gap must be kept smaller than 4 mm to 5 mm in order to rely completely on the results of this analysis. Regarding the leakage, which is the most important parameter in the performance of a dc-break, it has been found that, in the case of WR-62 waveguides, operating at 14.4 GHz, a dc-break with 1 mm gap, loaded by teflon, will have as much as 33% leakage. This result imposes a detailed design of a choke-flange, which must be used in the junction of the two waveguides to reflect back the radiation coming out from the gap, even at low-power operating levels.


## ACKNOWLEDGMENTS

The authors wish to thank Dr. G. Mourier of Thomson Tubes Electroniques for many valuable discussions. One of the authors (C.T.I) warmly acknowledges the support received from the "Human Capital and Mobility" program of the European Economic Communities.

## APPENDIX

In this appendix we will present the detailed calculations for the integrals $I_{nm}$ and $J_{nm}$ given by (31a) and (31b)

$$I_{nm} = -d \int_{-\infty}^{+\infty} \frac{dk_y}{2\pi} \frac{\cot\left(d\sqrt{k'^2 - k_y^2}\right)}{d\sqrt{k'^2 - k_y^2}} \int_0^a dy \cos(k_{ym}y) e^{jk_y y} \int_0^a dy' \cos(k_{ym}y') e^{-jk_y y'}$$

$$J_{nm} = -\frac{d}{2} \int_{-\infty}^{+\infty} \frac{dk_y}{2\pi} \frac{\csc\left(d\sqrt{k'^2 - k_y^2}\right)}{d\sqrt{k'^2 - k_y^2}} \int_0^a dy \cos(k_{ym}y) e^{jk_y y} \int_0^a dy' \cos(k_{ym}y') e^{-jk_y y'}$$

In the computation that follows we will consider that the relative dielectric constant $\epsilon_r$ is a complex quantity given by

$$\epsilon_r = \epsilon_r + j\eta$$

where $\eta$ corresponds to damping as the waves propagate along the dielectric waveguide, and $\epsilon_r$ is the dielectric constant of the medium filling up the waveguide.

First we will perform the integration with respect to $k_y$

$$\int_{-\infty}^{+\infty} dk_y \frac{\cot\left(d\sqrt{k'^2 - k_y^2}\right)}{d\sqrt{k'^2 - k_y^2}} e^{j(y-y')k_y} \tag{A1}$$

$$\int_{-\infty}^{+\infty} dk_y \frac{\csc\left(d\sqrt{k'^2 - k_y^2}\right)}{d\sqrt{k'^2 - k_y^2}} e^{j(y-y')k_y} \tag{A2}$$

using the methods of contour integration in the complex plane, and considering $k_y$ as a complex quantity. First of all, we observe that the functions $\cot(d\sqrt{k'^2 - k_y^2})$ and $\csc(d\sqrt{k'^2 - k_y^2})$ are not analytic everywhere in the complex plane. Indeed, they have poles at

$$k_y = \pm k'$$

and

$$k_y = \pm jk_\ell = \pm j\sqrt{\frac{\ell^2\pi^2}{d^2} - k'^2}$$

where $\ell = 1, 2, 3, \ldots$. Physically, the poles $k_y = \pm k'$ correspond to the $TE_{10}$ mode, while the $k_y = \pm jk_\ell$ correspond to the $TE_{1\ell}$ and $TM_{1\ell}$ modes, that can be generated in the dielectric waveguide.

For the $\cot(d\sqrt{k'^2 - k_y^2})$ function the residue of the $k'$ poles is found to be

$$R(\pm k') = \mp \frac{1}{2k'd^2} e^{j(y-y')k'} \tag{A3}$$

while that of the $k_\ell$ poles is given by

$$R(\pm jk_\ell) = \mp j \frac{1}{k_\ell d^2} e^{(y-y')k_\ell} \tag{A4}$$

For the $\csc(d\sqrt{k'^2 - k_y^2})$ function the residue of the $k'$ poles remain the same, while that of the $k_\ell$ poles is given by

$$R(\pm jk_\ell) = \mp j \frac{(-1)^\ell}{k_\ell d^2} e^{(y-y')k_\ell} \tag{A5}$$

Since the integrands of (A1) and (A2) contain an exponential dependence on $k_y$ of the form

$$e^{j(y-y')k_y}$$

we have to choose how to close the contour of integration according to the sign of the quantity $y - y'$. If $y - y' > 0$ we have to close the contour of integration in the upper-half complex plane (see Fig.10a), while in the opposite case $y - y' < 0$ the contour has to be closed in the lower-half complex plane, as it is shown in Fig.10b. In each case we enclose one propagating mode pole. Using the residue theorem, we obtain the following results

$$\int_{-\infty}^{+\infty} dk_y \frac{\cot\left(d\sqrt{k'^2 - k_y^2}\right)}{d\sqrt{k'^2 - k_y^2}} e^{j(y-y')k_y} = -\frac{\pi}{d^2}\left[j\frac{1}{k'}e^{j(y-y')k'} + \sum_{\ell=1}^{\infty}\frac{2}{k_\ell}e^{(y-y')k_\ell}\right] \tag{A6}$$

for the upper-half plane $(y - y' > 0)$, and

$$\int_{-\infty}^{+\infty} dk_y \frac{\cot\left(d\sqrt{k'^2 - k_y^2}\right)}{d\sqrt{k'^2 - k_y^2}} e^{j(y-y')k_y} = -\frac{\pi}{d^2}\left[j\frac{1}{k'}e^{-j(y-y')k'} + \sum_{\ell=1}^{\infty}\frac{2}{k_\ell}e^{-(y-y')k_\ell}\right] \tag{A7}$$

for the lower-half plane $(y - y' < 0)$.

To carry out the integrations with respect to $y$ and $y'$, we proceed in the following way. Since we have different expressions for the integrals (A1) and (A2) in different domains of $y$ and $y'$, we divide the square domain from $y = 0$ to $y = a$ and from $y' = 0$ to $y' = a$, into two triangular domains; in the triangular domain (I) of the $yy'$ plane (see Fig.11), the quantity $y - y'$ is always positive, while in the second domain (II), the quantity $y - y'$ is always negative. Thus, we break the surface integral on $yy'$ of (A1) and (A2) into two sub-integrals to be performed in the above described triangular domains (I) and (II), by substituting expressions (A6) and (A7), respectively, into (A1) and (A2). The limits of integration in domain (I) are from $y' = 0$ to $y' = y$ and then from $y = 0$ to $y = a$, while in the second domain (II) the limits are from $y = 0$ to $y = y'$ and from $y' = 0$ to $y' = a$.

Then, the integral $I_{nm}$ takes the form

$$I_{nm} = j\frac{1}{2k'd}\left(I^{\mathrm{I}}_{nm} + I^{\mathrm{II}}_{nm}\right) + \sum_{\ell=1}^{\infty}\frac{1}{k_\ell d}\left(I^{\mathrm{I}}_{nm\ell} + I^{\mathrm{II}}_{nm\ell}\right) \qquad (A8)$$

where

$$I^{\mathrm{I}}_{nm} = \int_0^a dy\cos(k_{ym}y)\int_0^y dy'\cos(k_{yn}y')e^{j(y-y')k'}$$

$$I^{\mathrm{II}}_{nm} = \int_0^a dy'\cos(k_{yn}y')\int_0^{y'} dy\cos(k_{ym}y')e^{-j(y-y')k'}$$

$$I^{\mathrm{I}}_{nm\ell} = \int_0^a dy\cos(k_{ym}y)\int_0^y dy'\cos(k_{yn}y')e^{-(y-y')k_\ell}$$

and

$$I^{\mathrm{II}}_{nm\ell} = \int_0^a dy'\cos(k_{yn}y')\int_0^{y'} dy\cos(k_{ym}y)e^{(y-y')k_\ell}$$

An expression similar to (A8) holds for the $J_{nm}$ integral.

Since the above integrals to be performed on $y$ and $y'$ are trivial, we may present only the final result given in eqns.(32) and (33).

## REFERENCES


[1] G. L. Ragan, *Microwave Transmission Circuits.* McGraw-Hill, New York, 1948.

[2] N. Marcuvitz, *Waveguide Handbook.* McGraw-Hill, New York, 1951.

[3] R. Geller, "Electron Ion Heating in ECRIS", *Proceedings of the 11th International Workshop on Electron Cyclotron Resonance Ion Sources (ECRIS 11)*, ed. A. G. Drentje, University of Gröningen, The Netherlands, pp. 1-17, May 6-7, 1993.

[4] V. Bechtold, H. Dohrmann and S. A. Sheikh, "A Highly Efficient ECR Ion Source for Radioactive Beams", *Contributed paper of the 7th Workshop on ECR Ion Sources*, ed. H. Beuscher, KernForschungAnlage Jülich, Germany, pp. 248-260, May 22-23, 1986.

[5] B. Jacqout, P. Briand F. Bourg and R. Geller, "Sources d'ions lourds caprice 10GHz $2\omega_{ce}$", *Nucl. Instrum. and Methods* **A269**, pp. 1-6, 1988.

[6] R. Geller, "Electron cyclotron resonance (E.C.R.) multiply charged ion sources", *IEEE Trans. Nucl. Science*, **NS26**, pp. 2120-2127, 1979.

[7] M. Cavenago and G. Bisoffi, "Optimization studies of a 14.4 GHz ECR ion source for the superconductive linac at Legnaro", *Nucl. Instrum. Methods* **A301**, pp. 9-18, 1991.

[8] M. Cavenago and G. Bisoffi, "The Legnaro ECR ion source", *Rev. Sci. Instrum.*, **63**, 4, pp. 2857-2859, 1992.

[9] G. Mourier, "Electromagnetic fields in cylindrical waveguides and cavities with sources", private communication.

[10] M. Cavenago and C. T. Iatrou, "Microwave components in the ECR Alice and a model for plasma impedance", *LNL-INFN-REP, Laboratori Nazionali di Legnaro*, Internal Report, in preparation.

## FIGURE CAPTIONS

1. Rectangular waveguide.
2. The infinite parallel-plates waveguide model.
3. The cross-section of the waveguide model and the metallic boundaries.
4. Reflected, transmitted, and radiated power versus the width of the gap with a dielectric constant $\epsilon_r = 2.1$.
5. As in Fig.4 with the $k_1$ poles excluded.
6. As in Fig.4 with the $\Phi$-function's coefficients excluded.
7. Reflected, transmitted, and radiated power versus the dielectric constant with a gap width $d = 1$ mm.
8. As in Fig.7 with the $\Phi$-function's coefficients excluded.
9. As in Fig.7 with the $k_1$ poles excluded.
10. Poles and integration contour in the complex plane.
11. Domains of integration in the $yy'$ plane.

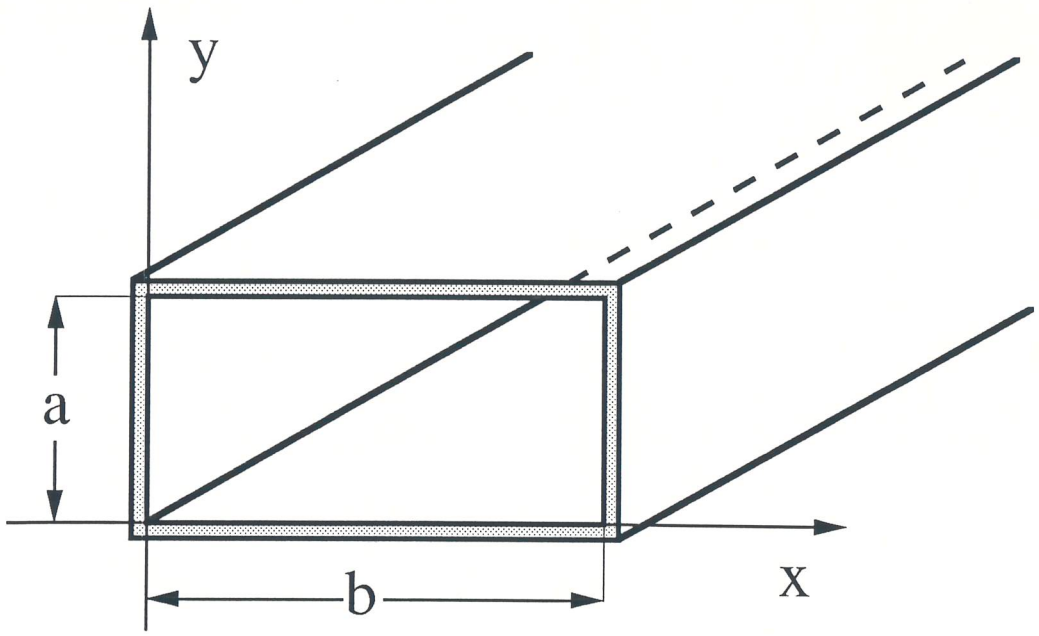


Fig 1: Rectangular waveguide

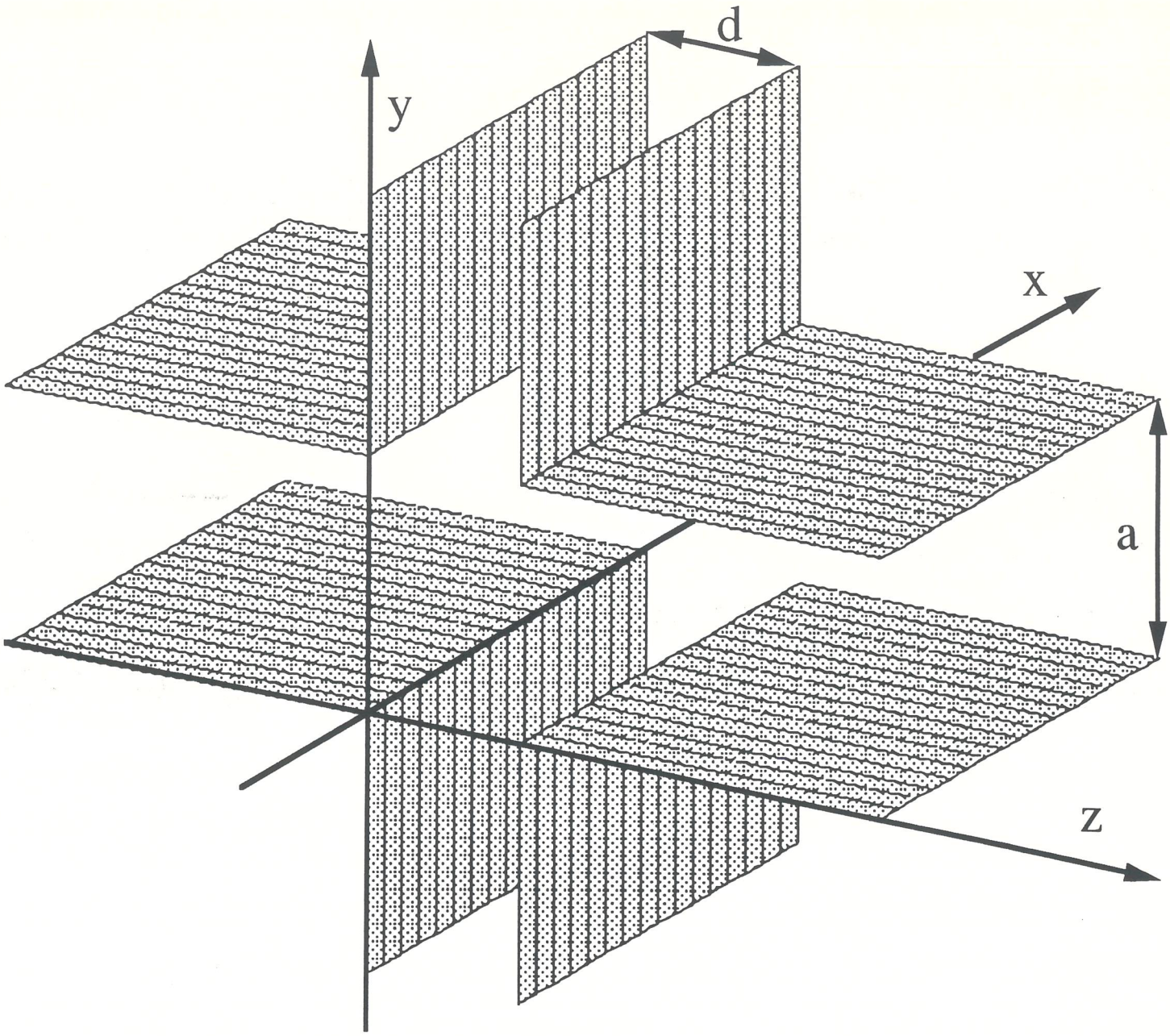


2. The infinite parallel-plates waveguide model.

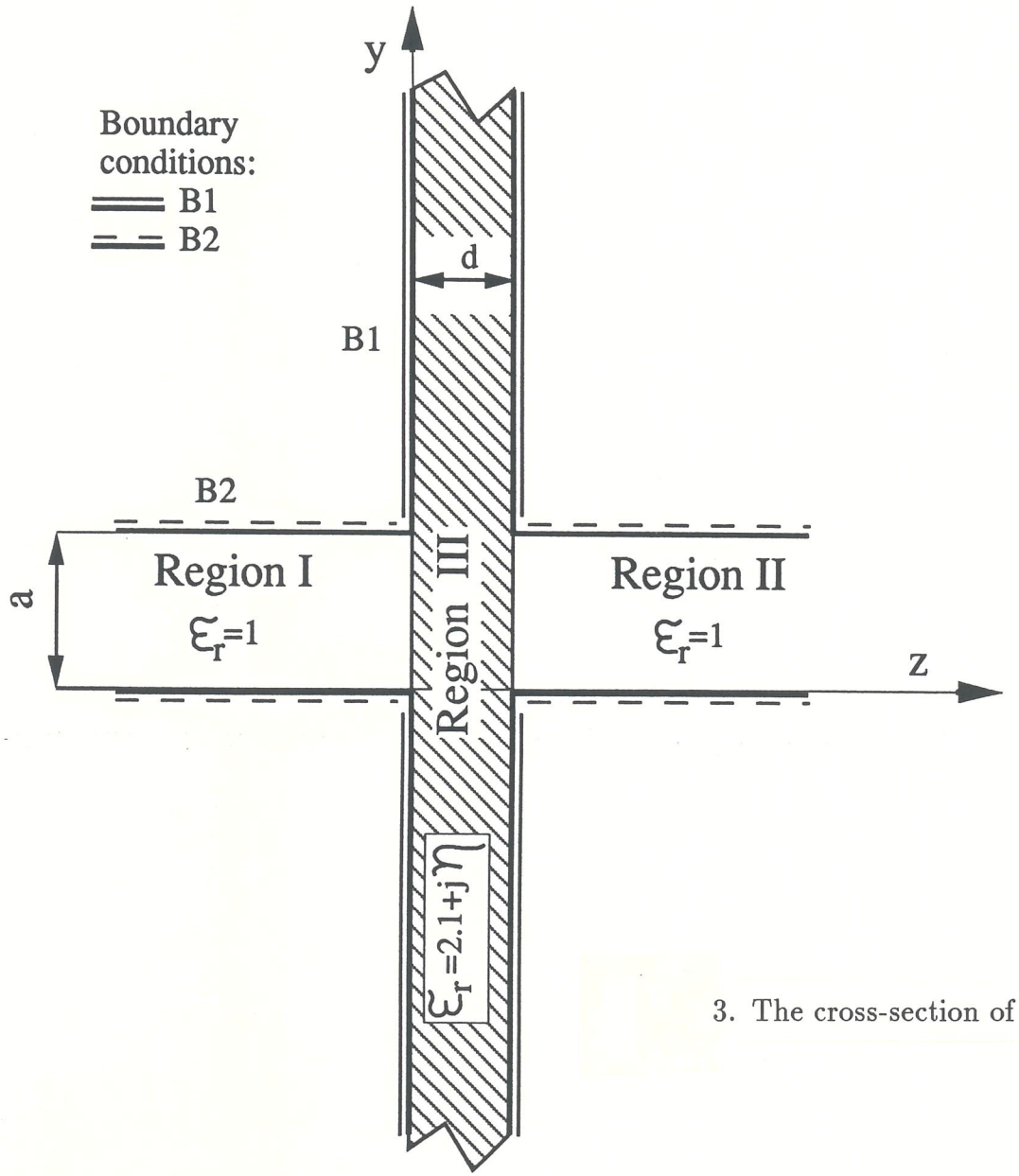


3. The cross-section of the waveguide model and the metallic boundaries.

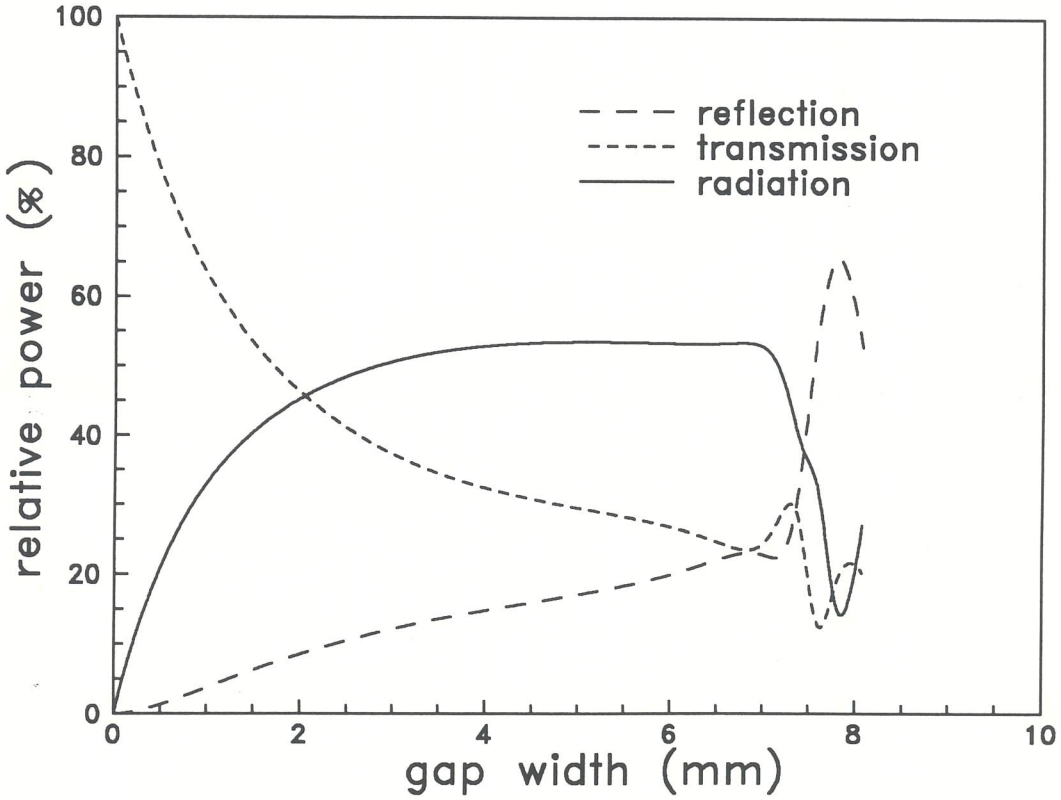


4. Reflected, transmitted, and radiated power versus the width of the gap with a dielectric constant $\epsilon_r = 2.1$.

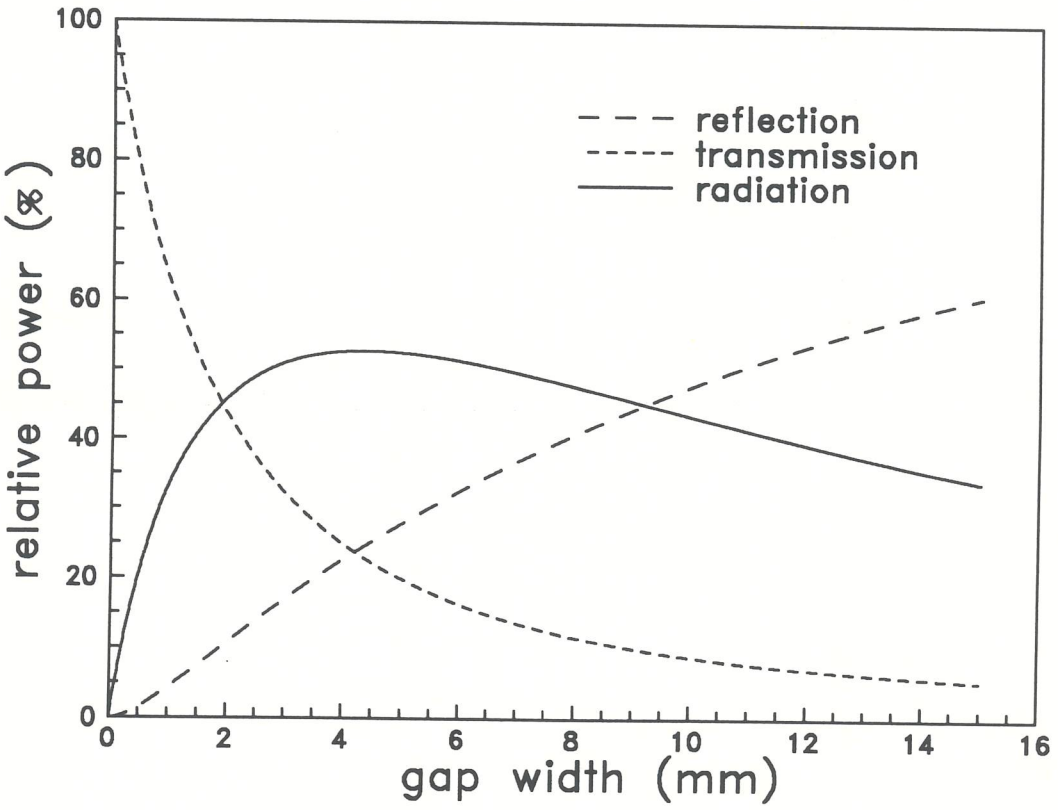


5. As in Fig.4 with the $k_1$ poles excluded.

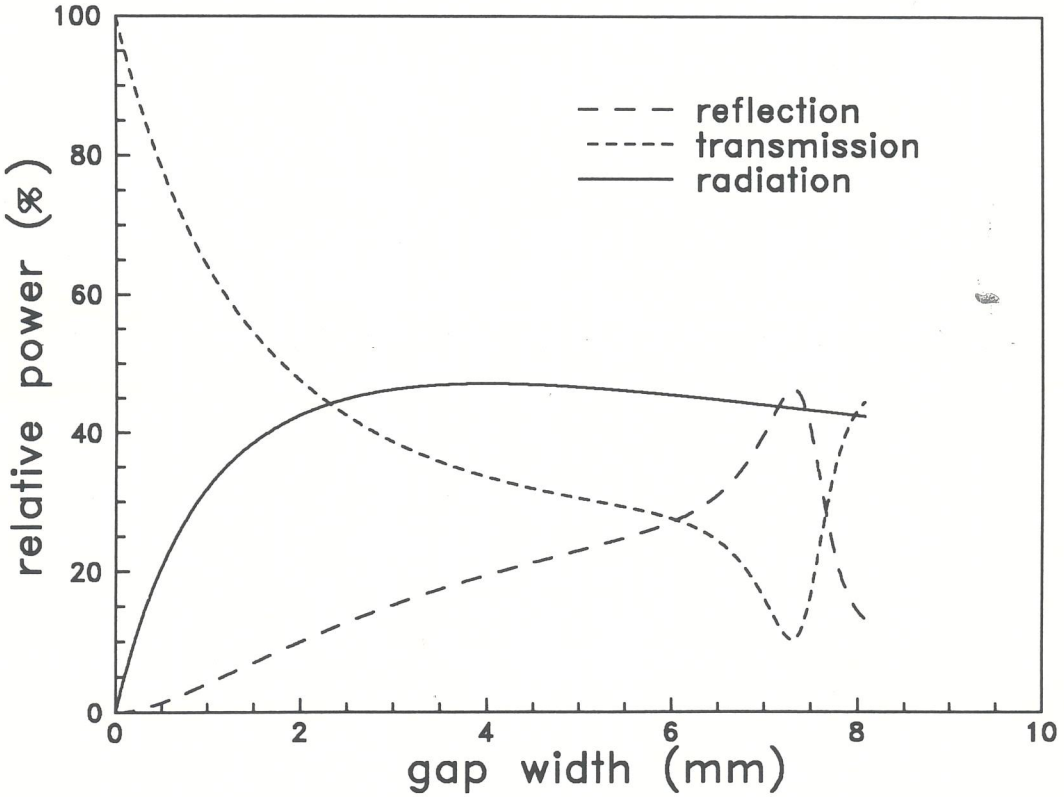


6. As in Fig.4 with the Φ-function's coefficients excluded.

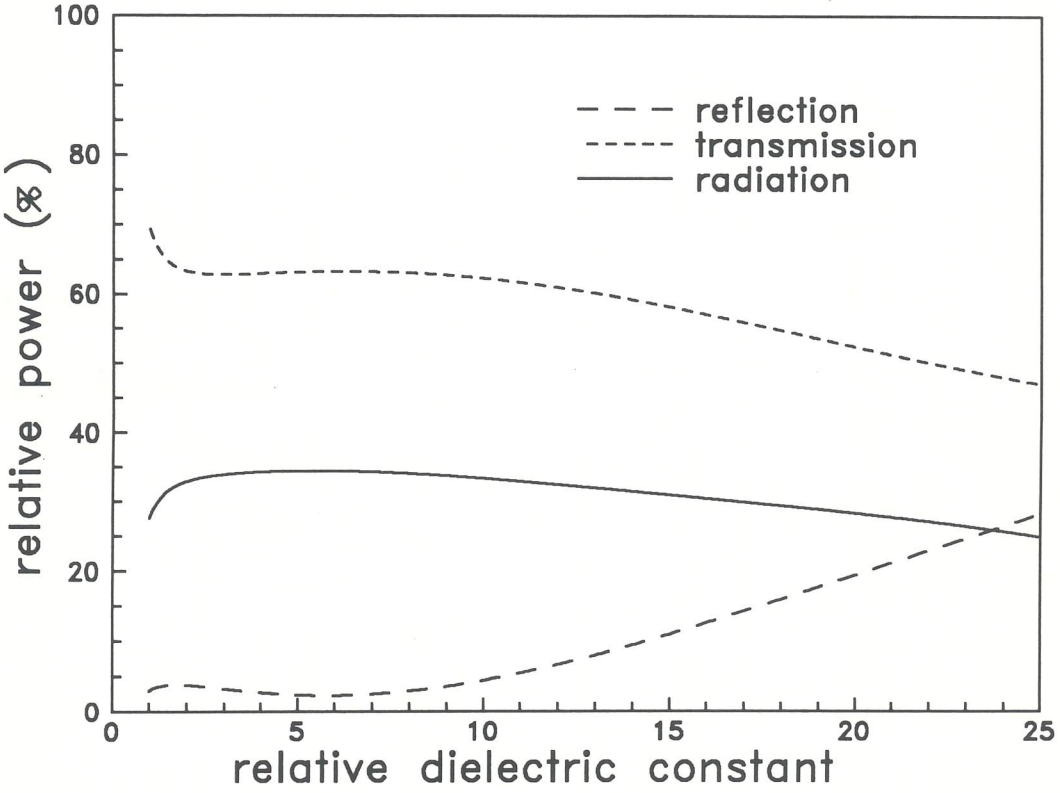


7. Reflected, transmitted, and radiated power versus the dielectric constant with a gap width $d = 1$ mm.

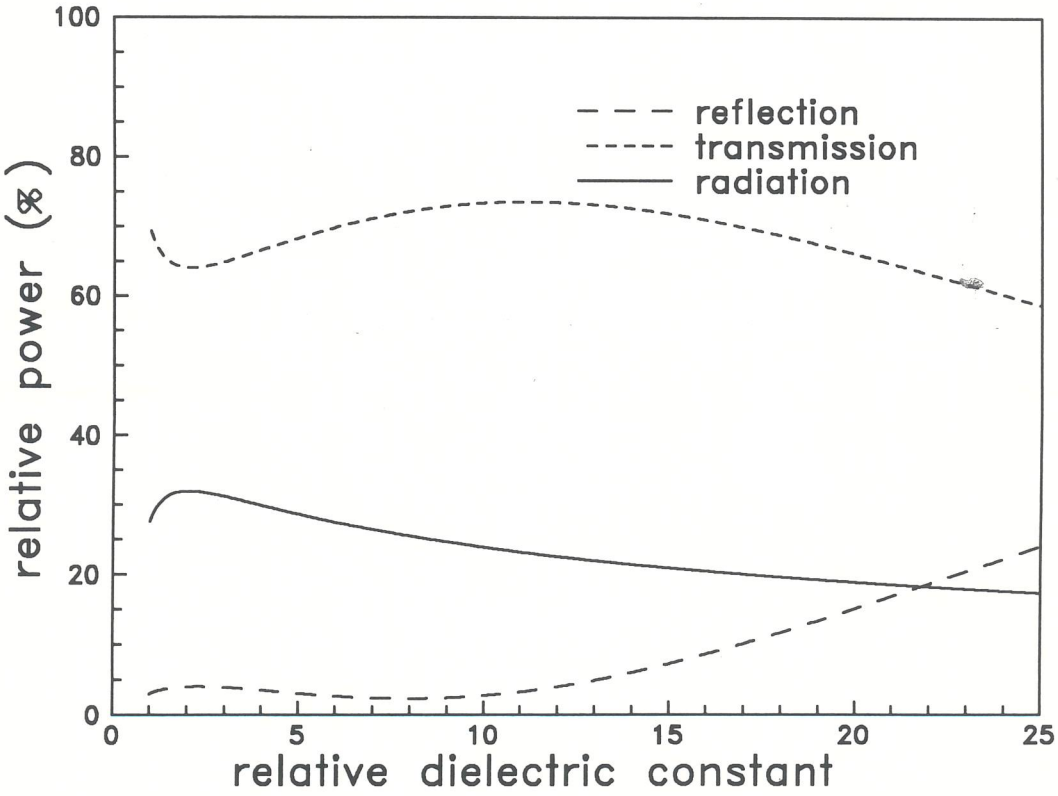


8. As in Fig.7 with the Φ-function's coefficients excluded.

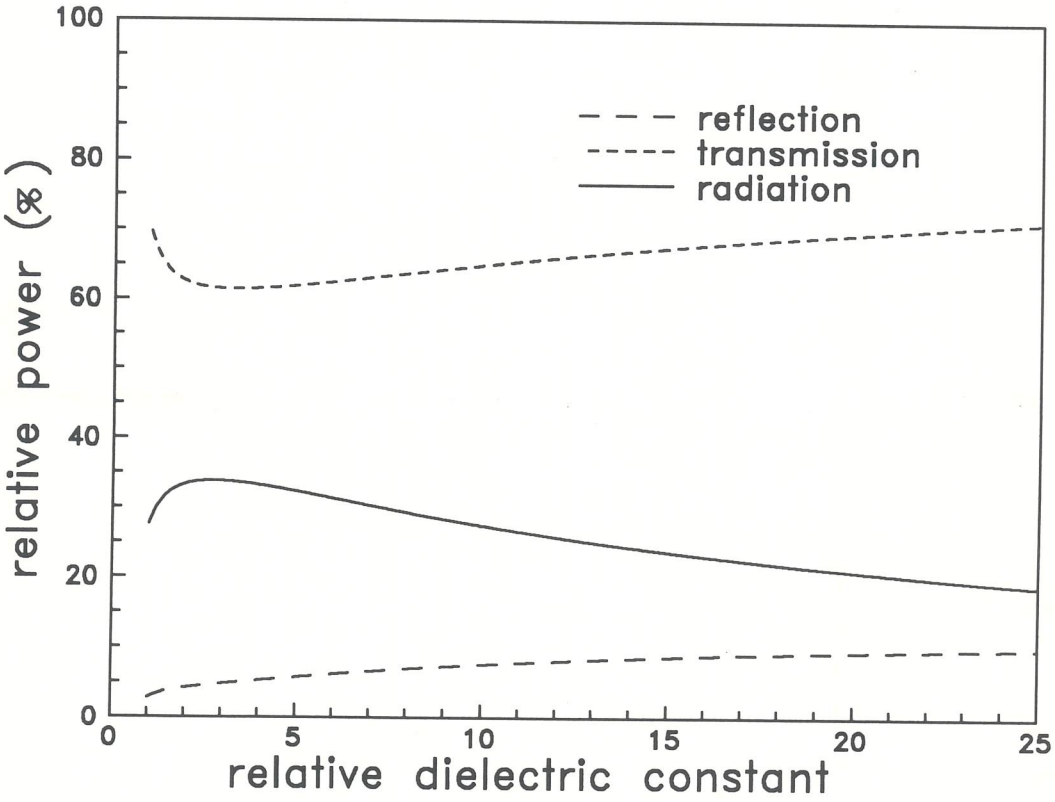


9. As in Fig.7 with the $k_1$ poles excluded.

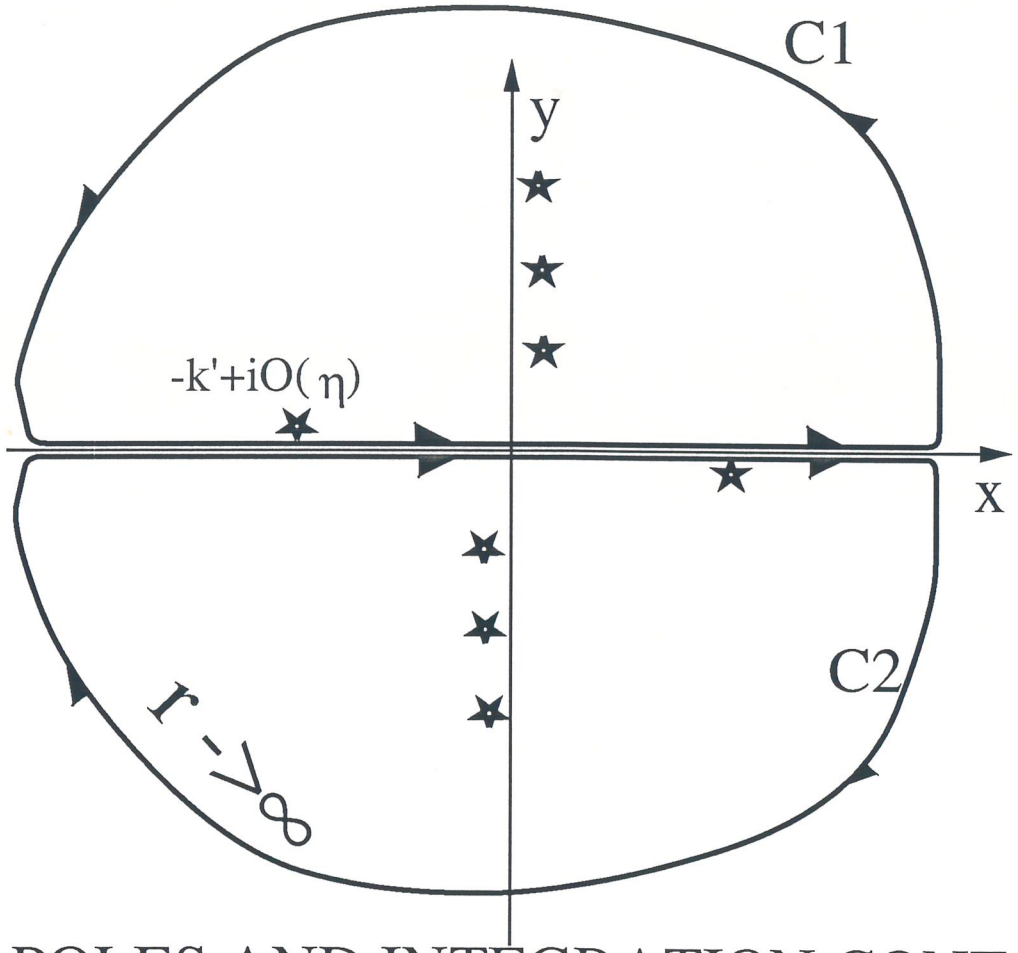


FIG 10 : POLES AND INTEGRATION CONTOURS

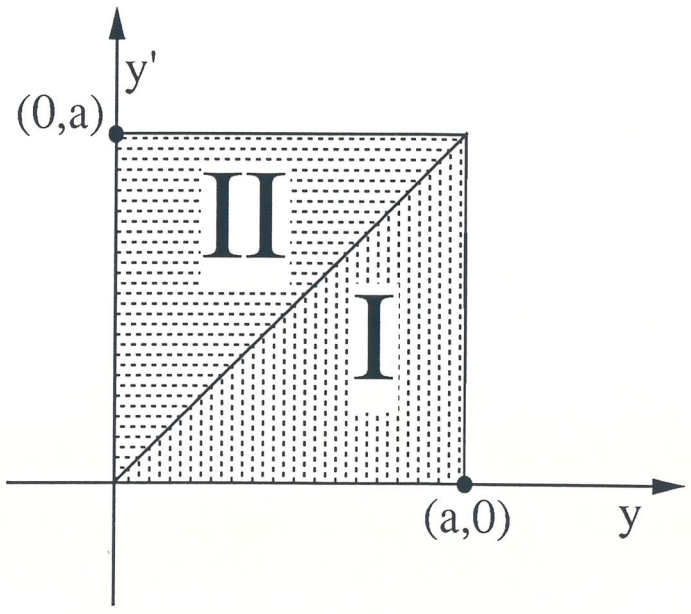


FIG 11: Domains of integration in yy' plane